Nanoscale

ROYAL SOCIETY OF CHEMISTRY

COMMUNICATION

Cite this: *Nanoscale*, 2020, **12**, 2980

Received 29th December 2019,
Accepted 7th January 2020

DOI: 10.1039/c9nr10930g

rsc.li/nanoscale

Unravelling the formation mechanism of alkynyl protected gold clusters: a case study of phenylacetylene stabilized Au_{144} molecules†

Xiaoshuang Ma, [a] Zhenghua Tang, *[a,b] Lubing Qin,[a] Jin Peng,[a] Ligui Li [a] and Shaowei Chen *[c]

Despite recent progress in the preparation of alkynyl protected Au clusters with molecular purity (*e.g.*, $Na[Au_{25}(C{\equiv}CAr)_{18}$, Ar = 3,5-$(CF_3)_2C_6H_3^-$, $Au_{36}(C{\equiv}CPh)_{24}$, $Au_{44}(C{\equiv}CPh)_{28}$, and $Au_{144}(C{\equiv}CAr)_{60}$, Ar = 2-F-$C_6H_4^-$), the formation mechanism still remains elusive. Herein, a new molecule-like alkynyl Au cluster was successfully prepared, and its formula was determined as $Au_{144}(PA)_{60}$ (PA = PhC≡C–, phenylacetylene). In the formation of $Au_{144}(PA)_{60}$, the introduction of ethanol in post-synthesis treatment to manipulate the aggregation state of the precursor was found to play a critical role in producing the Au144 clusters. During the $Au_{144}(PA)_{60}$ formation process, the contents of PA, $(PA)_2$ and $(PA)_4$ were monitored by absorbance and gas chromatography-mass spectrometry (GC-MS), disclosing that $Au_{144}(PA)_{60}$ molecules were generated in sync with $(PA)_4$. Finally, the formation mechanism of $Au_{144}(PA)_{60}$ molecules has been tentatively proposed, of which three major stages are involved. This study can shed light on the formation mechanism that may be exploited for the precise control of the synthesis of alkynyl protected coinage metal clusters.

Introduction

Molecular Au clusters protected by an organic capping layer exhibit unique optical, electronic, and magnetic properties,[1–12] and can find applications in diverse fields, such as catalysis,[13–16] medicine,[17,18] surface patterning[19,20] and optoelectronics.[21–23] In prior research, Au clusters were mostly protected by phosphines and thiolates. More recently, acetylene derivatives have emerged as a new capping ligand for nanoparticle surface functionalization. Unlike the phosphine and thiolate ligands, the –C≡C– group of an alkynyl ligand can function as both a σ donor and a π donor when coordinated to a metal core, which imparts significantly different physical, chemical and electronic properties to the Au clusters,[24,25] as compared to the phosphine and thiolate counterparts. For instance, Tsukuda *et al.* prepared a series of organogold clusters protected by phenylacetylene (PA), including $Au_{54}(PA)_{26}$, $Au_{94}(PA)_{38}$, and $Au_{110}(PA)_{40}$ in Au : (C≡CPh) mixture clusters,[26] and subsequently investigated the bonding motif between the teminal alkynes and Au clusters.[27] In another study, Kobayashi *et al.* reported the crystal structure of $[Au_8(dppp)_4(C{\equiv}CR)_2]^{2+}$ (dppp = 1,3-bis(dipheny-phosphino) propane), the first phosphine-coordinated molecular Au clusters having alkynyl substituents.[28] Later on, Wang and coworkers determined the crystal structure of alkynyl protected $Au_{36}(C{\equiv}CPh)_{24}$ and $Au_{44}(PhC{\equiv}C)_{28}$ clusters,[29] which was the first report on homoleptic alkynyl protected Au clusters with atomic precision. Lei *et al.* subsequently reported the progress with $Au_{144}(C{\equiv}CAr)_{60}$ (Ar = 2-F-$C_6H_4^-$).[30] Note that it represents the largest molecular alkynyl Au cluster ever documented so far. Recently, the total structure of the long-pursued alkynyl-protected Au_{25} clusters ($Na[Au_{25}(C{\equiv}CAr)_{18}]$, Ar = 3,5-$(CF_3)_2C_6H_3^-$) has been successfully determined,[31] which delivers a stong message that there is a similar but quite different parallel alkynyl-protected metal cluster universe in comparison with the thiolated ones.

Notably, the family of homoleptic alkynyl protected Au clusters remains very limited, which include only $Au_{25}L_{18}$, $Au_{36}L_{24}$, $Au_{44}L_{28}$, $Au_{54}L_{26}$ and $Au_{144}L_{60}$ (L = –C≡CR). One main reason is that the widely employed Brust–Schiffrin synthesis[32,33] and ligand exchange or etching approach[6,34] are effective for preparing thiolate capped molecular Au clusters but cannot be

[a]*Guangzhou Key Laboratory for Surface Chemistry of Energy Materials and New Energy Research Institute, School of Environment and Energy, South China University of Technology, Guangzhou Higher Education Mega Center, Guangzhou, Guangdong, 510006, P. R. China. E-mail: zhht@scut.edu.cn*

[b]*Guangdong Engineering and Technology Research Center for Surface Chemistry of Energy Materials, School of Environment and Energy, South China University of Technology, Guangzhou Higher Education Mega Centre, Guangzhou, Guangdong, 510006, P. R. China*

[c]*Department of Chemistry and Biochemistry, University of California, 1156 High Street, Santa Cruz, California, 95064, USA. E-mail: shaowei@ucsc.edu*

†Electronic supplementary information (ESI) available: Experimental details, supporting figures and tables. CCDC 1904135 for $(PA)_4$. For ESI and crystallographic data in CIF or other electronic format see DOI: 10.1039/c9nr10930g

directly adopted for the preparation of the alkynyl counterparts. In addition, despite the success of the production of molecular alkynyl Au clusters,[29,30,35–40] there is a lack of fundamental understanding regarding the formation process. Note that in the classic $Au_{25}(SC_2H_4Ph)_{18}$ synthesis, the aggregation state of the Au(I) : SR intermediate is found to play a crucial role in the formation of $Au_{25}(SC_2H_4Ph)_{18}$ at high yields.[41] Then, will the composition and aggregation state of the Au(I)-alkynyl complex precursor impact the synthesis of molecular alkynyl Au clusters, too? How can one manipulate these? What is the exact formation pathway? These questions form the aim and motivation of the current investigation.

Herein, we report the synthesis of molecular PA-capped Au144 clusters. The thiolate Au144 cluster was first captured by Whetten's group using laser desorption ionization mass spectrometry (LDI-MS) in 1996.[42,43] Jin's group conducted a high-yield exclusive synthesis, and its precise composition was determined as $Au_{144}(SR)_{60}$ by using electrospray mass spectrometry (ESI-MS) in 2009.[44] For more than two decades, the precise structural information of Au144 clusters was missing. As mentioned in the above paragraph, in 2018, Wang and coworkers reported the total structure of the first alkynyl-protected $Au_{144}(C{\equiv}CAr)_{60}$ (Ar = 2-F-$C_6H_4^-$) cluster, which consists of a Au_{54} two-shelled Mackay icosahedron enclosed by a Au_{60} anti-Mackay icosahedral shell.[30] Recently, Wu's study regarding the atomic structure of thiolate protected Au144 clusters also showed a similar Au core architeture.[45] In this study, the PA-capped Au clusters were prepared, and the formula was determined as $Au_{144}(PA)_{60}$ by ESI-MS. In the formation of $Au_{144}(PA)_{60}$ clusters, it was found that the introduction of ethanol in post-synthesis treatment to form a special flower-like precursor (denoted as $(Au–PA)_f$ hereafter) is critical for yielding Au144 clusters. During the $Au_{144}(PA)_{60}$ formation process, the contents of PA, $(PA)_2$ and $(PA)_4$ were monitored by absorbance and GC-MS, and $Au_{144}(PA)_{60}$ molecules were produced in sync with $(PA)_4$. Finally, the formation mechanism of $Au_{144}(PA)_{60}$ clusters has been tentatively proposed, of which three major stages are involved.

Results and discussion

Characterization of the $(Au–PA)_f$ precursor

The specific Au–PA precursor was first prepared by following the previously documented protocol with some modifications (more discussion in the section of characterization of the precursor), and the detailed synthesis route is illustrated in Scheme S1.† In a previous study,[29] Wang's group used acetone as the solvent to prepare an Au–PA precursor for the eventual generation of molecular $Au_{44}(PA)_{28}$ and $Au_{36}(PA)_{24}$ clusters. Since the solvent can affect the aggregation state of the Au–PA precursor which likely impacts the size of the final Au clusters, in this work ethanol was introduced in post-synthesis treatment to produce the specific $(Au–PA)_f$ precursor (see the ESI† for more details). In comparison with acetone, ethanol possesses higher surface tension and polarity, which can be employed as a desolvation solvent to manipulate the aggregation state of the precursor.

SEM measurement was first performed to observe the surface morphology of the $(Au–PA)_f$ precursor. Fig. 1 presents the typical SEM images of the $(Au–PA)_f$ precursor in comparison with the reported Au–PA precursor. As illustrated in Fig. 1a and b, randomly dispersed amorphous sheet-like structures with various sizes can be easily identified for Au–PA, while in sharp contrast, well-defined flowers are evenly distributed for $(Au–PA)_f$, and each flower possessed a diameter of approximately 20–25 μm (Fig. 1c). Interestingly, the homogeneous flowers consisted of plenty of regular needle-like petals (Fig. 1d). Such a huge morphological difference between the two precursors attests that ethanol indeed impacted the aggregation state of the precursor profoundly.

Subsequently, the powder X-ray diffraction measurement was conducted to examine the crystal structure difference between the Au–PA precursor and the $(Au–PA)_f$ precursor. As shown in Fig. 1e, for Au–PA, with 2θ values ranging from 10.0° to 45.0°, there are two broad peaks with 2θ located at 14.63° and 29.99°, suggesting that an amorphous structure with a complicated composition is probably obtained. However, for $(Au–PA)_f$, sharp peaks with strong signals can be easily identified. This might be because the introduction of ethanol could alter the desolvation effects of acetone through hydrogen bonding and hence can lead to the formation of some homo-

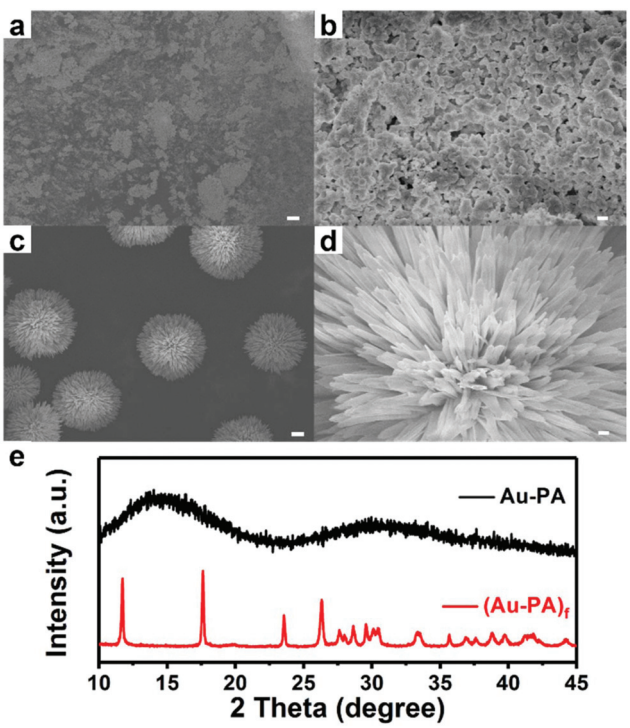

Fig. 1 Typical SEM image of the Au–PA precursor (a) 5 μm, (b) 500 nm and the $(Au–PA)_f$ precursor (c) 5 μm, (d) 500 nm, respectively. (e) Powder XRD spectra of the randomly aggregated Au–PA precursor (without EtOH) and the specially aggregated $(Au–PA)_f$ precursor (with EtOH, this work).

geneous precursor with a certain aggregation state. Particularly, when the 2θ value is below 20°, from the 2θ at 11.81° and 17.65°, the inter-phase spacing of 7.48 Å, and 5.02 Å can be deduced. The presence of 2θ at 23.59° and 26.26° is probably caused by the strong π–π interactions of the benzene rings in PA molecules, that is, there are two face-to-face stacking patterns with a distance of 3.39 Å and 3.77 Å, respectively.[46] In addition, there are some other peaks with relatively low intensity in the 2θ range from 27.63° to 44.24° (d = 2.04 to 3.23 Å), which can be attributed to the Au–Au aurophilic interaction, Au–C≡C bonding and some other possible inter-phase spacings.[46]

Fig. S1† shows the FTIR spectra of the $(Au–PA)_f$ and Au–PA precursors.[29,35] One can see that the –C≡C– stretching appeared at 2008 cm^{-1} with Au–PA, but blue-shifted to 2054 cm^{-1} with $(Au–PA)_f$. This suggests somewhat weakened π-bonding between metal d-orbitals and the phenylethynyl π_g-orbital in the latter that allowed for a faster growth and eventually generating large-sized Au clusters.[47,48] Such finding is in good accordance with the fact that large-sized clusters of Au144 were acquired in this study.

Compositional determination of $Au_{144}(PA)_{60}$ molecules

To determine the composition of the purified Au clusters, the final product was analyzed by electrospray ionization mass spectrometry.[49] As presented in Fig. 2a, its formula can be determined to be $Au_{144}(PA)_{60}$ (cal: 34 430.87 g mol^{-1}, exp: 34 430.00 g mol^{-1}), and the mass peaks of 4+, 3+, and 2+ (in source ionization) were observed. Thermogravimetric analysis (TGA) was then conducted (Fig. 2b), where a total weight loss of 17.87% was observed. From the Au : PA mass ratio, the formula of the Au cluster can be further confirmed as $Au_{144}(PA)_{60}$ (calculated Au : PA mass ratio 82.34 : 17.66).

The electronic structure of $Au_{144}(PA)_{60}$ was subsequently probed by X-ray photoelectron spectroscopy (XPS) measurements. The survey scan spectra of $Au_{144}(PA)_{60}$ is shown in Fig. 2c, in which the key elements of Au and C can be identified. Fig. 2d presents the core-level Au 4f spectra of $Au_{144}(PA)_{60}$ and $(Au–PA)_f$. It can be noted that the binding energy of the Au $4f_{7/2}$ electrons in $Au_{144}(PA)_{60}$ is 83.9 eV, which is in the intermediate between the documented Au(0) and Au(I) values;[50,51] and this energy is somewhat lower (*ca.* 0.21 eV) than that in $(Au–PA)_f$, consistent with the formation of a packed gold core. In addition, based on the integrated peak area, the Au : C atomic ratio is estimated to be 1 : 3.3 (Table S1†), in good agreement with the theoretical value of 1 : 3.1. Furthermore, the Au(I) : Au(0) atomic ratio was *ca.* 1 : 3.9, consistent with the value of 1 : 3.8 observed with $Au_{144}(PA)_{60}$ (Table S2†). Taken together, these results indicate that $Au_{144}(PA)_{60}$ and $Au_{144}(C{\equiv}CAr)_{60}$ (Ar = 2-F-$C_6H_4^-$) most likely adopted the same gold core scaffold.

Fourier-transform infrared (FTIR) measurements were then performed to obtain structural insights into the metal–ligand interfacial bonds in $Au_{144}(PA)_{60}$. From Fig. S2,† the absence of the ≡C–H vibrational band indicates the direct bonding between the alkynyl carbon and the gold core in $Au_{144}(PA)_{60}$. Furthermore, the –C≡C– stretching of PA (2110 cm^{-1})[52,53] is found to red-shift to 2028 cm^{-1} in $Au_{144}(PA)_{60}$, mostly because when the alkynyl carbon was bound covalently to gold atoms, the –C≡C– bond was weakened by electron transfer from the Au core to the π* orbital of the acetylene moiety.[54,55]

UV-visible absorbance of the $Au_{144}(PA)_{60}$ clusters

Fig. 3 shows the UV-visible absorption spectrum of the $Au_{144}(PA)_{60}$ clusters, which features an exponential-decay profile, along with four discrete peaks located at *ca.* 399 nm (3.11 eV), 452 nm (2.74 eV), 542 nm (2.29 eV), and 631 nm (1.97 eV). Note that the spectral characteristics of $Au_{144}(PA)_{60}$

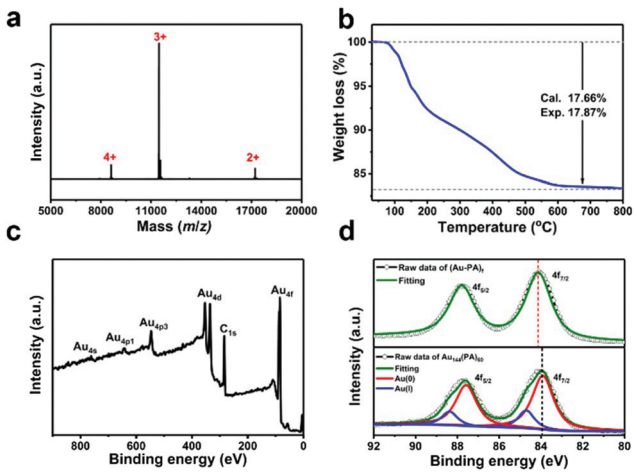

Fig. 2 (a) Electrospray ionization mass spectrometry (ESI-MS) characterization of $Au_{144}(PA)_{60}$. The peaks correspond to the 4+, 3+, and 2+ ion sets of $Au_{144}(PA)_{60}$. (b) TGA curve of the $Au_{144}(PA)_{60}$ clusters. (c) XPS survey scan spectra of the $Au_{144}(PA)_{60}$ clusters. (d) Core-level XPS spectra of the Au 4f electrons in $Au_{144}(PA)_{60}$ and $(Au–PA)_f$. Black curves are experimental data, green curves show the fitting results. For the Au 4f core-level XPS spectra of $Au_{144}(PA)_{60}$, the red line denotes the deconvoluted Au(0) species, while the blue line denotes the deconvoluted Au (I) species. The binding energy was calibrated based on the C 1s peak at 284.6 eV.

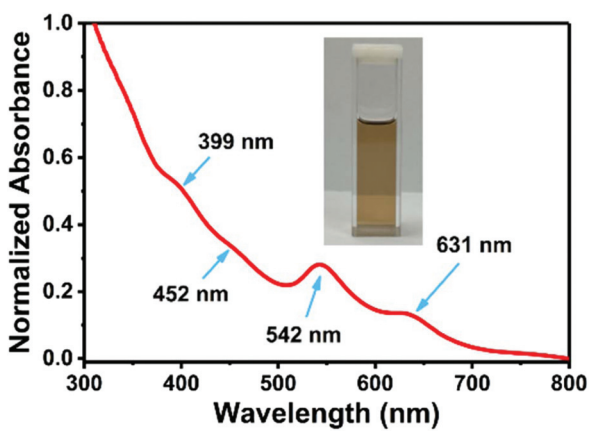

Fig. 3 Absorbance spectrum of the $Au_{144}(PA)_{60}$ clusters in CH_2Cl_2 (inset shows the as-purified Au cluster solution).

are significantly different from that of $Au_{144}(SR)_{60}$,[44,45] suggesting a strong ligand effect on the optical properties between the thiolate ligand and alkynyl ligand. Moreover, compared with $Au_{144}(C{\equiv}CAr)_{60}$ (Ar = 2-F-$C_6H_4^-$),[30] the absorbance profile of $Au_{144}(PA)_{60}$ also shows some slight differences (*e.g.* 560 nm and 620 nm for $Au_{144}(C{\equiv}CAr)_{60}$ *vs.* 542 nm and 631 nm for $Au_{144}(PA)_{60}$), implying that the *m*-position F in the phenyl ring of the ligand holds discernible perturbation on the absorbance of the Au144 clusters.

The *in situ* monitoring of the content change of PA, $(PA)_2$, and $(PA)_4$

Given the complexity of the Au(I)-alkynyl precursor, the unpredictability to manipulate the reduction process and the lack of *in situ* advanced characterization tools, it has been mostly a black box regarding the formation mechanism of the emerging alkynyl protected Au clusters. Thus, it is of fundamental interest to study the reaction kinetics from the $(Au–PA)_f$ precursor to $Au_{144}(PA)_{60}$. Upon the addition of $NaBH_4$, the reaction mixture was monitored by capillary gas chromatography-mass spectrometry (GC-MS) at different time intervals. As shown in Fig. 4a, two peaks can be observed at a retention time of *ca.* 4 min and *ca.* 21 min, respectively. They were determined as PA and $(PA)_2$ by MS measurement (Fig. 4b), respectively. Monomeric PA remained visible for up to 4 h after the addition of $NaBH_4$, but vanished at 12 h. Additional PA ligands were added into the solution at this time, and after additional 24 h (36 h in total), the amount of PA can be seen to decrease (Fig. 4a). Meanwhile, the amount of $(PA)_2$ increased in the first 12 h; however, after the addition of more PA ligands at 12 h, the amount of $(PA)_2$ decreased gradually. This is caused by the formation of $(PA)_4$ (more discussion below, Fig. 4c).

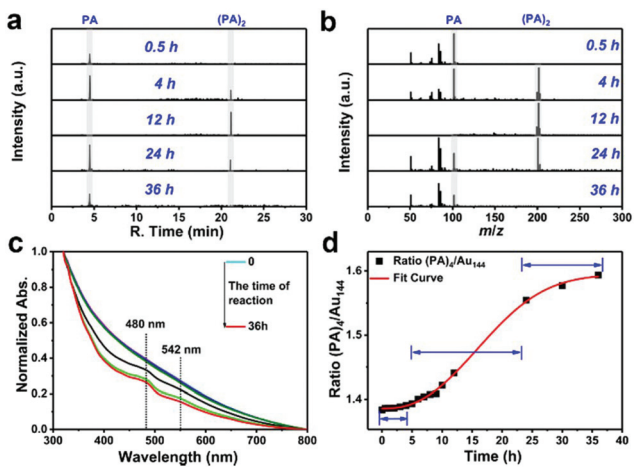

Fig. 4 (a) Gas chromatography *vs.* time regarding the content change of PA and $(PA)_2$ at different times (0.5 h, 8 h, 12 h, 24 h, 36 h) during the formation of the $Au_{144}(PA)_{60}$ clusters. (b) Corresponding mass spectrum of PA and $(PA)_2$ at different times. (c) The absorbance change acquired after the addition of $NaBH_4$ at different time intervals (0 h, 0.5 h, 1 h, 2 h, 3 h, 4 h, 5 h, 6 h, 7 h, 8 h, 12 h, 24 h, and 36 h). An aliquot of the reaction mixture in the methylene chloride phase was diluted to the proper absorbance range for each measurement. The spectra were normalized at 320 nm. (d) Time-dependent absorbance change (ratio $(PA)_4/Au_{144}$) of $(PA)_4$ (480 nm) relative to Au_{144} (542 nm).

The absorbance change of the reaction mixture was simultaneously monitored, as shown in Fig. 4c. For up to 36 h, the absorbance peak at 480 nm became gradually intensified, which was accompanied by the enhancement of the signal at 542 nm (the fingerprint absorbance peak of $Au_{144}(PA)_{60}$). Fig. S3a† presents the absorbance spectra of $(PA)_4$, where a broad peak at 480 nm can be easily recognized. Furthermore, the crystal structure of $(PA)_4$ can be found in Fig. S3b,† where the detailed structural parameters for $(PA)_4$ are summarized in Table S3.† Interestingly, $(PA)_4$ holds a cumulene structure, and the cumulene skeleton was first revealed in 1994.[56] Cumulene is an important intermediate in the organic synthesis regime, and it can be prepared in the presence of metal catalysts.[57] Note that, this is the first-ever observation that cumulene as byproduct was produced during the formation of alkynyl Au clusters. Using the absorbance values at 480 nm and 542 nm as the metric of $(PA)_4$ and $Au_{144}(PA)_{60}$, the relative $(PA)_4$-to-$Au_{144}(PA)_{60}$ ratio can be approximately quantified (Fig. 4c). Basically, there are roughly three periods (Fig. 4d). In the initial 4 h, the molecular ratio of $(PA)_4$-to-$Au_{144}(PA)_{60}$ remained approximately constant (Fig. S4a†), as only a small amount of $(PA)_4$ and $Au_{144}(PA)_{60}$ were produced. In the second period (4 h–24 h) (Fig. S4b†), this ratio increased sharply, indicating $(PA)_4$ and $Au_{144}(PA)_{60}$ emerged simultaneously and the amount of $(PA)_4$ and $Au_{144}(PA)_{60}$ increased concurrently. Finally, in the last 12 h, the ratio gradually became stable, suggesting a dynamic balance was eventually reached (Fig. S4c†). At 36 h, the amount of both $(PA)_4$ and $Au_{144}(PA)_{60}$ reached the maximal point and remained stable. Further extension of the reaction time would not generate more $Au_{144}(PA)_{60}$ clusters, as the absorbance profiles at 36 h and 48 h overlapped completely (Fig. S5†).

Proposed $Au_{144}(PA)_{60}$ formation mechanism

Based on the above results, a tentative mechanism from the $(Au–PA)_f$ precursor to form $Au_{144}(PA)_{60}$ is proposed and illustrated in Scheme 1. It involves three major stages. Firstly, upon the addition of $NaBH_4$, polydisperse Au clusters protected by PA were formed with the release of free PA ligands. Such a process (Stage I) occurred in the first 4 h and can be summarized in eqn (1):

$$(Au–PA)_f \rightarrow Au_{n_1}(PA)_{m_1} + (PA)_{free} \quad (1)$$

Subsequently, free PA ligands formed the $(PA)_2$ dimer, while the core-size of the Au clusters grew, as depicted in eqn (2):

$$Au_{n_1}(PA)_{m_1} + (PA)_{free} \rightarrow Au_{n_2}(PA)_{m_2} + (PA)_2 \quad (n_2 > n_1,\ m_2 > m_1) \quad (2)$$

This process occurred in the following 8 h (Stage II). At 12 h, the amount of $(PA)_2$ reached the maximal value while free PA ligands were totally exhausted, as observed in Fig. 4a and b. Additional PA ligands were introduced at this time point, and in the following 24 h (Stage III), the $(PA)_4$ tetramer

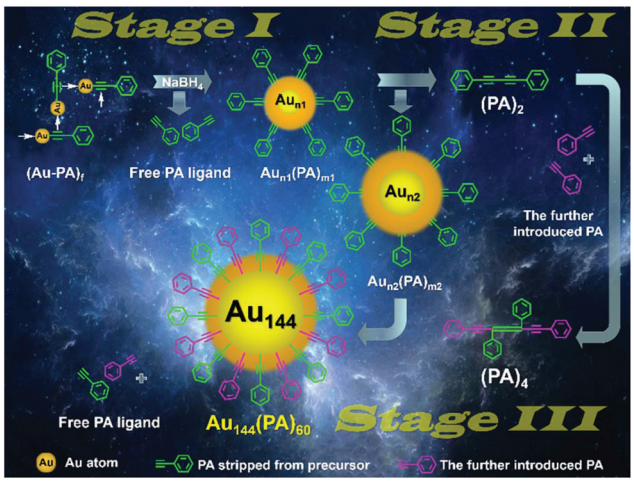

Scheme 1 The proposed formation mechanism of molecular $Au_{144}(PA)_{60}$ from the $(Au-PA)_f$ precursor.

formed while the polydisperse Au clusters evolved into $Au_{144}(PA)_{60}$ molecules eventually. The amount of $(PA)_4$ significantly increased during this final stage, and the maximal amount of molecular $Au_{144}(PA)_{60}$ clusters were generated. This process can be summarized in eqn (3):

$$Au_{n_2}(PA)_{m_2} + (PA)_2 \rightarrow Au_{144}(PA)_{60} + (PA)_4 \quad (3)$$

Conclusions

In conclusion, a new homoleptic alkynyl ligand PA protected molecular Au cluster formulated as $Au_{144}(PA)_{60}$ has been synthesized. Compared with $Au_{144}(SR)_{60}$ and $Au_{144}(C{\equiv}CAr)_{60}$, the structure of the PA ligand impacts strong perturbation to the electronic properties of the $Au_{144}(PA)_{60}$ molecules. During the synthesis, the introduction of ethanol in post-synthesis treatment is critical to form the desired $(Au-PA)_f$ precursor which eventually yielded $Au_{144}(PA)_{60}$ clusters. $Au_{144}(PA)_{60}$ molecules were produced in sync with the PA tetramer $(PA)_4$. Combining the above results, the formation mechanism of $Au_{144}(PA)_{60}$ has been tentatively proposed. This study can shed light on future rational design for preparing homoleptic alkynyl protected molecular coinage metal clusters.

Experimental section

Synthesis of the $(Au-PA)_f$ precursor

The $(Au-PA)_f$ precursor was prepared according to a reported protocol with some modifications.[36] In a typical synthesis, Me_2SAuCl (120.0 mg, 0.41 mmol) and PhC≡CH (66.3 μL, 0.61 mmol) were co-dissolved in acetone (15 mL) under ultrasonic treatment at room temperature (160 W, 40 kHz). After 10 min, Et_3N (83.6 μL, 0.61 mmol) was added under stirring (1000 rpm). The reaction mixture was kept under stirring at room temperature for 1 h in the absence of light. After the reaction was complete, the volume of the mixture was evaporated to 5 mL and 50 times excess (250 mL) ethanol was added dropwise (at intervals of 30 min, divided into four times, proportion of 1 : 2 : 2 : 4) with slight stirring (200 rpm) to give a light yellow solid (~80 mg), which was successively washed with ethanol (2 × 10 mL), water (2 × 10 mL), dry diethyl ether (3 × 10 mL) to remove PhC≡CH and dimethyl sulfoxide.

Synthesis of $Au_{144}(PA)_{60}$ clusters

The $Au_{144}(PA)_{60}$ clusters were prepared by direct reduction of the $(Au-PA)_f$ precursor with $NaBH_4$. Briefly, $(Au-PA)_f$ (50.00 mg, 0.17 mmol) was dispersed in dichloromethane (20 mL) under ultrasonic treatment (160 W, 40 kHz) at room temperature. After 10 min, a freshly prepared $NaBH_4$ (0.03 mmol in 1.0 mL of ethanol) solution was added dropwise (in 10 min) under stirring (800 rpm). The solution color changed from yellow to pale brown and finally to dark brown. The reaction mixture was kept under stirring at room temperature overnight in the absence of light. After 12 h, excess PhC≡CH (200 μL) and Et_3N (200 μL) were added into the mixture and the reaction was aged for one day under ambient temperature. After that, the volume of the mixture was evaporated to 4 mL and 50 times excess (200 mL) *n*-hexane was added to give a black solid, which was washed with excess *n*-hexane and collected by centrifugation. The crude products dissolved in 1 mL of CH_2Cl_2 were pipetted onto ten pieces of a preparative thin layer chromatography (PTLC) plate (10 cm by 20 cm), and the separation was conducted in a developing tank (solvent: CH_2Cl_2/*n*-hexane/Et_3N = 100 : 20 : 0.72, volume ratio) for ~10 min. Then, the band of $Au_{144}(PA)_{60}$ in the PTLC plate was cut, and the nanoclusters were extracted with pure CH_2Cl_2 and then dried by rotary evaporation.

Conflicts of interest

There are no conflicts to declare.

Acknowledgements

Z. T. acknowledges the financial support from the National Natural Science Foundation of China (No. 21501059), Guangdong Natural Science Funds for Distinguished Young Scholars (No. 2015A030306006), Guangzhou Science and Technology Plan Projects (No. 201804010323), the fundamental funds for central universities (SCUT No. 2018ZD022), as well as Guangdong Innovative and Entrepreneurial Research Team Program (No. 2014ZT05N200). S. C. thanks the National Science Foundation for partial support of the work (CHE-1710408 and CBET-1848841).

Notes and references

1 R. C. Jin, C. J. Zeng, M. Zhou and Y. X. Chen, *Chem. Rev.*, 2016, **116**, 10346–10413.

2 X. Kang, H. Chong and M. Zhu, *Nanoscale*, 2018, **10**, 10758–10834.
3 J. Z. Yan, J. Zhang, X. M. Chen, S. Malola, B. Zhou, E. Selenius, X. M. Zhang, P. Yuan, G. C. Deng, K. L. Liu, H. F. Su, B. K. Teo, H. Hakkinen, L. S. Zheng and N. F. Zheng, *Natl. Sci. Rev.*, 2018, **5**, 694–702.
4 L. Liu and A. Corma, *Chem. Rev.*, 2018, **118**, 4981–5079.
5 Z. Gan, N. Xia and Z. Wu, *Acc. Chem. Res.*, 2018, **51**, 2774–2783.
6 Q. Yao, T. Chen, X. Yuan and J. Xie, *Acc. Chem. Res.*, 2018, **51**, 1338–1348.
7 S. Hossain, Y. Niihori, L. V. Nair, B. Kumar, W. Kurashige and Y. Negishi, *Acc. Chem. Res.*, 2018, **51**, 3114–3124.
8 P. Chakraborty, A. Nag, A. Chakraborty and T. Pradeep, *Acc. Chem. Res.*, 2018, **52**, 2–11.
9 K. R. Krishnadas, A. Baksi, A. Ghosh, G. Natarajan, A. Som and T. Pradeep, *Acc. Chem. Res.*, 2017, **50**, 1988–1996.
10 W. W. Xu, X. C. Zeng and Y. Gao, *Acc. Chem. Res.*, 2018, **51**, 2739–2747.
11 Y. Du, H. Sheng, D. Astruc and M. Zhu, *Chem. Rev.*, 2020, **120**, 526–622.
12 T. Higaki, Q. Li, M. Zhou, S. Zhao, Y. Li, S. Li and R. Jin, *Acc. Chem. Res.*, 2018, **51**, 2764–2773.
13 G. Li and R. Jin, *J. Am. Chem. Soc.*, 2014, **136**, 11347–11354.
14 R. Sardar, A. M. Funston, P. Mulvaney and R. W. Murray, *Langmuir*, 2009, **25**, 13840–13851.
15 Q. Wang, L. Wang, Z. Tang, F. Wang, W. Yan, H. Yang, W. Zhou, L. Li, X. Kang and S. Chen, *Nanoscale*, 2016, **8**, 6629–6635.
16 L. Wang, Z. Tang, W. Yan, H. Yang, Q. Wang and S. Chen, *ACS Appl. Mater. Interfaces*, 2016, **8**, 20635–20641.
17 K. Zheng, M. I. Setyawati, D. T. Leong and J. Xie, *ACS Nano*, 2017, **11**, 6904–6910.
18 D. A. Giljohann, D. S. Seferos, W. L. Daniel, M. D. Massich, P. C. Patel and C. A. Mirkin, *Angew. Chem., Int. Ed.*, 2010, **49**, 3280–3294.
19 W. P. Wuelfing, S. J. Green, J. J. Pietron, D. E. Cliffel and R. W. Murray, *J. Am. Chem. Soc.*, 2000, **122**, 11465–11472.
20 M. Aslam, I. S. Mulla and K. Vijayamohanan, *Langmuir*, 2001, **17**, 7487–7493.
21 X. Kang and M. Zhu, *Chem. Soc. Rev.*, 2019, **48**, 2422–2457.
22 X. Yuan, Z. Luo, Y. Yu, Q. Yao and J. Xie, *Chem. – Asian J.*, 2013, **8**, 858–871.
23 P. Schwerdtfeger, *Angew. Chem., Int. Ed.*, 2003, **42**, 1892–1895.
24 Z. Lei and Q.-M. Wang, *Coord. Chem. Rev.*, 2019, **378**, 382–394.
25 Z. Lei, X. K. Wan, S. F. Yuan, Z. J. Guan and Q. M. Wang, *Acc. Chem. Res.*, 2018, **51**, 2465–2474.
26 P. Maity, H. Tsunoyama, M. Yamauchi, S. Xie and T. Tsukuda, *J. Am. Chem. Soc.*, 2011, **133**, 20123–20125.
27 P. Maity, S. Takano, S. Yamazoe, T. Wakabayashi and T. Tsukuda, *J. Am. Chem. Soc.*, 2013, **135**, 9450–9457.
28 N. Kobayashi, Y. Kamei, Y. Shichibu and K. Konishi, *J. Am. Chem. Soc.*, 2013, **135**, 16078–16081.
29 X. K. Wan, Z. J. Guan and Q. M. Wang, *Angew. Chem., Int. Ed.*, 2017, **56**, 11494–11497.
30 Z. Lei, J. J. Li, X. K. Wan, W. H. Zhang and Q. M. Wang, *Angew. Chem., Int. Ed.*, 2018, **57**, 8639–8643.
31 J. J. Li, Z. J. Guan, Z. Lei, F. Hu and Q. M. Wang, *Angew. Chem.*, 2018, **58**, 1083–1087.
32 M. Brust, M. Walker, D. Bethell, D. J. Schiffrin and R. Whyman, *J. Chem. Soc., Chem. Commun.*, 1994, 801–802.
33 H. Qian, M. Zhu, U. N. Andersen and R. Jin, *J. Phys. Chem. A*, 2009, **113**, 4281–4284.
34 C. Zeng, Y. Chen, A. Das and R. Jin, *J. Phys. Chem. Lett.*, 2015, **6**, 2976–2986.
35 X. K. Wan, W. W. Xu, S. F. Yuan, Y. Gao, X. C. Zeng and Q. M. Wang, *Angew. Chem., Int. Ed.*, 2015, **54**, 9683–9686.
36 X. K. Wan, Q. Tang, S. F. Yuan, D. E. Jiang and Q. M. Wang, *J. Am. Chem. Soc.*, 2015, **137**, 652–655.
37 T. Higaki, C. Liu, C. Zeng, R. Jin, Y. Chen, N. L. Rosi and R. Jin, *Angew. Chem., Int. Ed.*, 2016, **55**, 6694–6697.
38 S. F. Yuan, P. Li, Q. Tang, X. K. Wan, Z. A. Nan, D. E. Jiang and Q. M. Wang, *Nanoscale*, 2017, **9**, 11405–11409.
39 T. Wang, W. H. Zhang, S. F. Yuan, Z. J. Guan and Q. M. Wang, *Chem. Commun.*, 2018, **54**, 10367–10370.
40 Z. J. Guan, J. L. Zeng, S. F. Yuan, F. Hu, Y. M. Lin and Q. M. Wang, *Angew. Chem., Int. Ed.*, 2018, **57**, 5703–5707.
41 M. Zhu, E. Lanni, N. Garg, M. E. Bier and R. Jin, *J. Am. Chem. Soc.*, 2008, **130**, 1138–1139.
42 R. L. Whetten, J. T. Khoury, M. M. Alvarez, S. Murthy, I. Vezmar, Z. Wang, P. W. Stephens, C. L. Cleveland, W. D. Luedtke and U. Landman, *Adv. Mater.*, 1996, **8**, 428–433.
43 T. G. Schaaff, M. N. Shafigullin, J. T. Khoury, I. Vezmar and R. L. Whetten, *J. Phys. Chem. B*, 2001, **105**, 8785–8796.
44 H. Qian and R. Jin, *Nano Lett.*, 2009, **9**, 4083–4087.
45 N. Yan, N. Xia, L. Liao, M. Zhu, F. Jin, R. Jin and Z. Wu, *Sci. Adv.*, 2018, **4**, eaat7259.
46 Z. Wu, Y. Du, J. Liu, Q. Yao, T. Chen, Y. Cao, H. Zhang and J. Xie, *Angew. Chem.*, 2019, **58**, 8139–8144.
47 G. E. Coates and C. Parkin, *J. Chem. Soc.*, 1962, 3220–3226, DOI: 10.1039/jr9620003220.
48 N. J. Long and C. K. Williams, *Angew. Chem., Int. Ed.*, 2003, **42**, 2586–2617.
49 T. Higaki, M. Zhou, K. J. Lambright, K. Kirschbaum, M. Y. Sfeir and R. Jin, *J. Am. Chem. Soc.*, 2018, **140**, 5691–5695.
50 Z. Tang, B. Xu, B. Wu, M. W. Germann and G. Wang, *J. Am. Chem. Soc.*, 2010, **132**, 3367–3374.
51 Z. Tang, D. A. Robinson, N. Bokossa, B. Xu, S. Wang and G. Wang, *J. Am. Chem. Soc.*, 2011, **133**, 16037–16044.
52 W. Chen, N. B. Zuckerman, X. W. Kang, D. Ghosh, J. P. Konopelski and S. W. Chen, *J. Phys. Chem. C*, 2010, **114**, 18146–18152.

53 S. Back, R. A. Gossage, G. Rheinwald, I. del Río, H. Lang and G. van Koten, *J. Organomet. Chem.*, 1999, **582**, 126–138.
54 P. Maity, T. Wakabayashi, N. Ichikuni, H. Tsunoyama, S. Xie, M. Yamauchi and T. Tsukuda, *Chem. Commun.*, 2012, **48**, 6085–6087.
55 M. Iwasaki, Y. Shichibu and K. Konishi, *Angew. Chem.*, 2019, **58**, 2443–2447.
56 J. Anthony, C. Boudon, F. Diederich, J. P. Gisselbrecht, V. Gramlich, M. Gross, M. Hobi and P. Seiler, *Angew. Chem., Int. Ed. Engl.*, 1994, **33**, 763–766.
57 M. Arrowsmith, M. R. Crimmin, M. S. Hill, S. L. Lomas, D. J. MacDougall and M. F. Mahon, *Organometallics*, 2013, **32**, 4961–4972.